

## DEVELOPMENT OF PRE-REPAIR MACHINING STRATEGIES FOR LASER-AIDED METALLIC COMPONENT REMANUFACTURING

Xinchang Zhang\*, Wenyuan Cui\*, Leon Hill\*, Wei Li\*, Frank Liou\*

\*Department of Mechanical & Aerospace Engineering, Missouri University of Science and  
Technology, Rolla, Missouri, 65409, USA

### Abstract

Remanufacturing worn metallic components can prolong the service life of parts that need frequent replacement but are extremely costly to manufacture, such as aircraft titanium components, casting dies. Additive manufacturing (AM) technology enables the repair of such valuable components by depositing filler materials at the worn area layer by layer to regenerate the missing geometry. In general, damaged parts would be inspected and pre-machined prior to material deposition to remove oil, residue, oxidized layers or defects located in inaccessible regions. Therefore, the motivation of this paper is to introduce pre-repair machining strategies for removing contaminated materials from damaged components and materials surrounding inaccessible defects to ensure that the target damage is repairable. The current research targets at common failures comprising surface indentations, erosion, corrosion, wear and cracking, and the machining strategies for each defect were proposed. Each strategy takes the 3D scanned damaged model as input and the cut-off volume around the defects is defined by using different approaches. Pre-repair machining toolpath and program were generated based on the defined cut-off volume and finally, damaged parts were machined using the proposed strategies.

**Keywords:** Pre-repair machining; Component repair; Defects; Additive manufacturing

### 1. Introduction

Aircraft components and casting dies are subjected to premature failure due to impact with foreign objects, thermal fatigue cracking, erosion, corrosion, wear, etc. For obtaining improved performance and mechanical properties in a wide temperature range, such components are usually made of expensive alloys, i.e., Titanium- or Nickel-based alloys. Besides, most casting dies are extremely high-priced as a result of their complicated structure and manufacturing costs. Therefore, regular maintenance and repair are necessary to prolong their service life.

Laser-assisted additive manufacturing (LAM) process for component repair has been becoming an effective candidate for part refurbishment due to its good fabricated material properties and solid bi-material bonding [1]–[3], feasibility of depositing a wide range of materials [4]–[9], high-accurate positioning and motion control using computer [10], [11], as well as easily control of processing parameters [12]–[14]. LAM can deposit material on damaged components with different materials to form functional structure [15], [16]. LAM has different names at various laboratories such as direct metal deposition (DMD), Laser Engineering Net Shaping (LENS), laser metal deposition (LMD), etc. The basic principle of such techniques is a solid freeform fabrication process which is characterized as a layer-by-layer deposition technology that can directly build near-net shape fully dense components from CAD drawings. For component repair, the laser beam

was scanned on the target damaged area to generate a melt pool while a powder stream is conjected into the melt pool. The injected power undergoes rapid melting and then solidifies on the damaged substrate when the layer jogs away. Layer by layer, the missing volume is reobtained. The shape of deposits is directly controlled by moving the substrate along a pre-defined pattern. It has been widely reported that LAM as a remanufacturing technique has shown great applications in automotive, aerospace and die casting industries [17]–[24].

It was reported in [25], [26] that an integrated remanufacturing process generally undergoes the following steps: (1) Pre-repair inspection and decision; (2) Additive patch extraction; (3) Subtractive patch extraction; and (4) Quality Inspection. This is a universal repair routine that applied to various metallic components with diverse defects.

(1) In detail, a damaged part will at first experience a complete inspection to assess the feasibility and economy of restoring it. Since there are a variety of defects such as cracks, dents, wear, erosion, distortion, etc., and possibility in locating at a wide range of positions, the inspection and decision making is highly a case to case basis. However, the crucial factors are limited which comprise accessibility of defects, the area of damage, the geometry of the base structure and post-repair machining possibility.

(2) When repair is scheduled, the repair volume of the part is then extracted to generate additive toolpath. Damage extraction is a key to guarantee a successful repair because the refilled volume is directly determined by the additive toolpath. This process usually requires creating the damaged model through 3D scanning and then conducting Boolean operation between the recreated damaged model with the nominal model. A few algorithms have been developed for regenerating the geometry of the worn-out area [11], [18], [25], [27], [28].

(3) Subtractive machining succeeds the additive process since the as-deposited part may have unsatisfied surface roughness and inaccurate dimensions.

(4) In quality inspection step, the remanufactured part is checked for any appearance of defects to ascertain that the repair is successful. In addition, the restored part is 3D scanned and then compared with the nominal model to catch possible dimensional distortion due to errors in damage extraction and heating /cooling introduced residual stress.

However, the abovementioned repair routine is not complete because, in general, worn components cannot be directly deposited without pre-repair machining. Ultrasonic cleaning or rinse can only remove surface oil or debris on worn parts but cannot remove materials surrounding inaccessible defects (such as cracks or defects in sharp corners) or contaminated materials on worn surfaces. Depositing materials on such regions cannot guarantee the interfacial bonding strength. Unsolid bonding could cause delamination when reputing the part into service. Contaminated inclusion of filler material and base decimates the mechanical properties and therefore leaves great threaten especially on key components such as aircraft turbine and compression blades. Therefore, this research introduced pre-repair machining before additive patch extraction to assure the repairability of the damaged part.

The aim of this paper is to develop pre-repair machining methodologies for component repair. The purpose of the proposed methodologies aims to benefit repair process by not only cutting off surrounding materials around inaccessible defects but also removing contaminated layers on worn parts. Because the cut-off volume must be redeposited, the removed volume in pre-repair machining should be minimized. The overall methodologies presented in this paper take the 3D scanned model as input and based on the types of defects, different machining strategies were proposed. This study targets three types of defects: (1) surface impact defects; (2) surface erosion, corrosion and wear; (3) Cracking. The methodology is an integrated structure of 3D digitization, machining volume extraction, and pre-machining program generation.

## **2. Pre-repair machining strategy for impact defects**

The pre-repair machining procedure for surface impact defects such as dents, notches, grooves and material overcut is illustrated in Fig. 1, which includes (1) Damaged part cleaning and pre-repair inspection; (2) Model reconstruction; (3) Cut-off volume definition; (4) Target geometry acquisition; (5) Pre-machining toolpath and NC code generation; and (6) Pre-repair machining. The procedure is summarized in this section and detailed discussed in sections 2.1 – 2.5.

In the beginning, the damaged part is throughout ultrasonic cleaned and inspected to determine the repair possibility. The inspection is mainly conducted by technicians due to the excess possible locations of damage. When pre-repair machining is needed, the model of the damaged part is then reconstructed. After that, the volume of material enveloping the damage is defined. Thereafter, the target geometry can be obtained. Subsequently, based on the target geometry, pre-machining toolpath and NC node can be generated. The NC code can be exported to the machining system for machining.

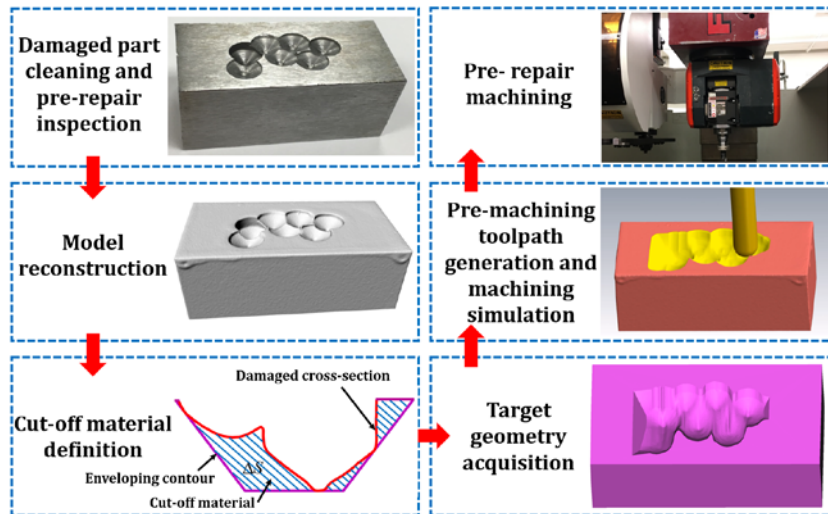


**Fig. 1** Pre-repair machining procedure for surface impact damage

### **2.1 Damaged part cleaning and pre-repair inspection**

An H13 tool steel block with dimensions of 50 mm × 25.4 mm × 25.4 mm was utilized as an example for illustrating pre-machining strategy of surface impact damage (Fig. 2). Ball-

indented defects were randomly prepared on the surface of the substrate using an 8 mm drill bit. The drilled holes on the block have varied depths and overlap ratios.

One can see in Fig. 2 that the damaged substrate cannot be repaired directly without pre-repair machining due to at least two reasons. One is that vertical surfaces on the side of the holes are not accessible to the laser beam and powder feed nozzle for 3-axis system. Directly depositing materials on such areas cannot guarantee the sound bi-material bonding. Therefore, materials surrounding vertical surfaces need to be machined to reveal a tilt surface to guarantee the accessibility. Another reason is that the rough tiny edges in the damaged area not only complicate the toolpath planning for material deposition but also may distort during deposition due to heat input that ruins the accuracy of deposited geometry. Therefore, it is necessary to machine off a certain amount of material enveloping the damage to provide a repairable geometry.

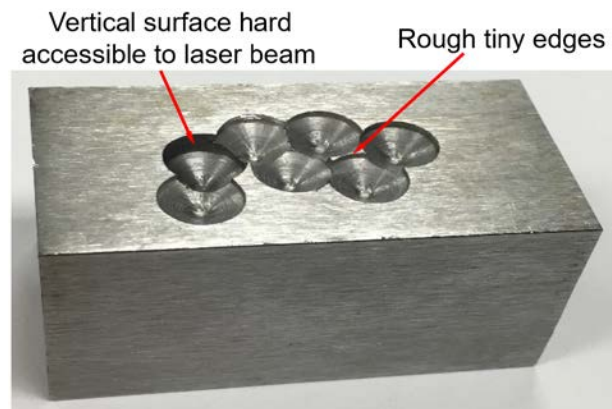


**Fig. 2** An H13 tool steel substrate with ball-indented damage on the top surface

## **2.2 Model reconstruction of damaged component with impact damage**

Recreating the model of worn part is required for planning the pre-repair machining. In this research, models of damaged parts were reconstructed using a structured-light optical 3D scanner (Shining3D OptimScan-5M, Fig. 3) that can yield a validated accuracy of 20  $\mu\text{m}$ . The scanner has a blue light projector that emits structured-light patterns on an object and two CCD cameras on the scanner measure the distorted dimensions of the pattern. The alteration in dimensions provides the three-dimensional coordinates of the object. In order to acquire a complete model, multiple scans are demanded for capturing different orientations of the object. For registering point cloud from different scans to a single model, indexing targets need to be randomly pasted around the object to be scanned. Fig. 4a depicts the point cloud of the substrate and the point cloud was further processed to create the STL model shown in Fig. 4b.

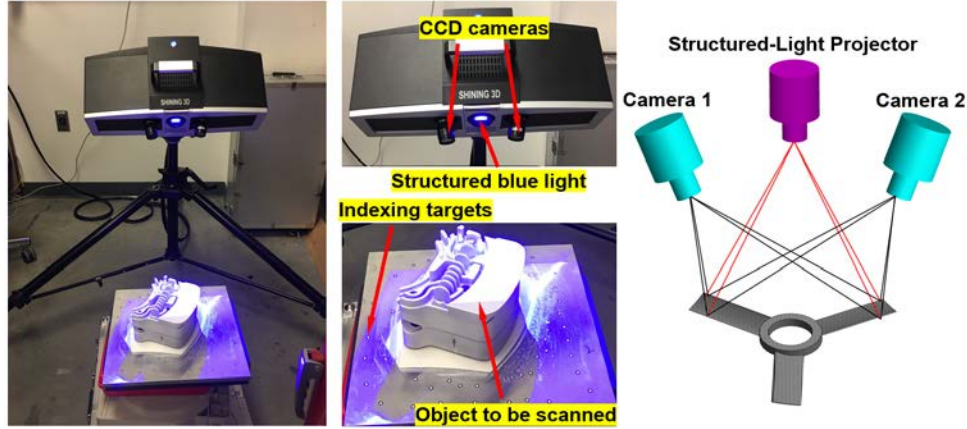


**Fig. 3** Shining 3D structured-light scanner for model reconstruction

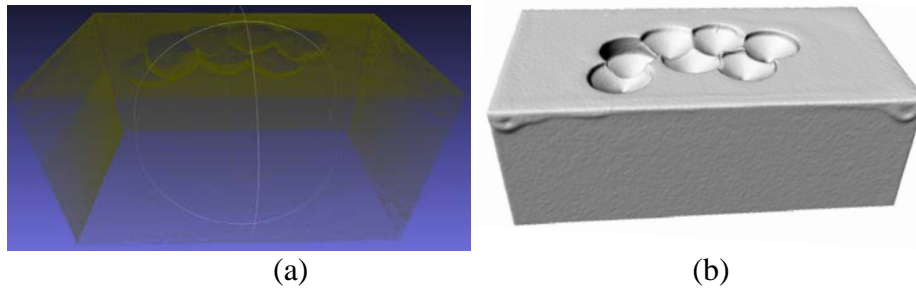


**Fig. 4** Point cloud (a) and reconstructed STL model (b) of the H13 tool steel block

### **2.3 Cut-off volume definition**

The STL model of the damaged part was sliced into a number of layers along the y-axis with a layer thickness of 0.5 mm as shown in Fig. 5a. The slicing outputs a series of layers that combined damaged and undamaged cross-sections. Damaged cross-sections also contain points in damaged and undamaged regions. Damaged points can be easily extracted by calculating the distance from the points to the nominal surface. A tolerance can be set so that points with distance beyond the tolerance would be defined as damaged points. Fig. 5b presents a cross-section where damage starts on the left and ends on the right.

In order to machine off materials around the defects, based on the damaged cross-sections, two enveloping boundaries, U-shaped boundary (Fig. 5b) and convex-hull boundary (Fig. 7a), were utilized. Both closed profiles contain the damaged area and surrounding materials to provide a good accessibility to the LAM system.

#### **2.3.1 U-shaped boundary definition**

As shown in Fig. 5b, for U-shaped contour, two approaching lines with an inclination angle  $\theta$  ( $PQ$  on the left and  $MN$  on the right) were utilized to approach the damaged cross-section. The damage starting point  $S(x_S, y_S, z_S)$  and ending point  $E(x_E, y_E, z_E)$  were known during the damaged point searching stage. It is necessary to find points  $P, Q, M,$  and  $N$  to define the two approaching lines. Once such points were determined, the U-shaped boundary can be obtained.

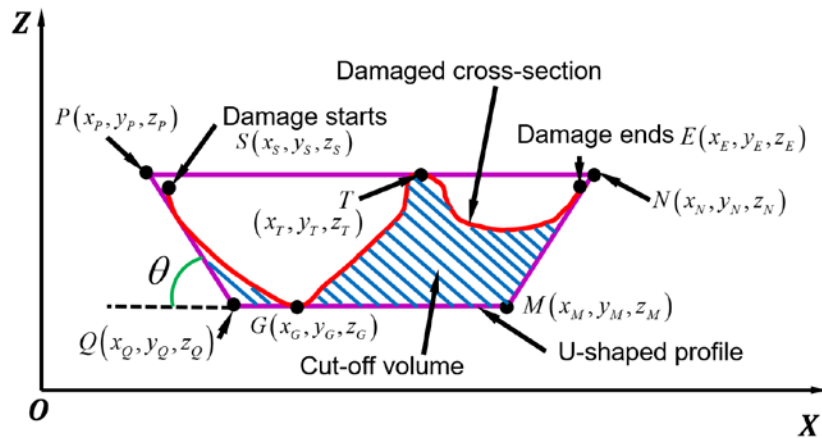
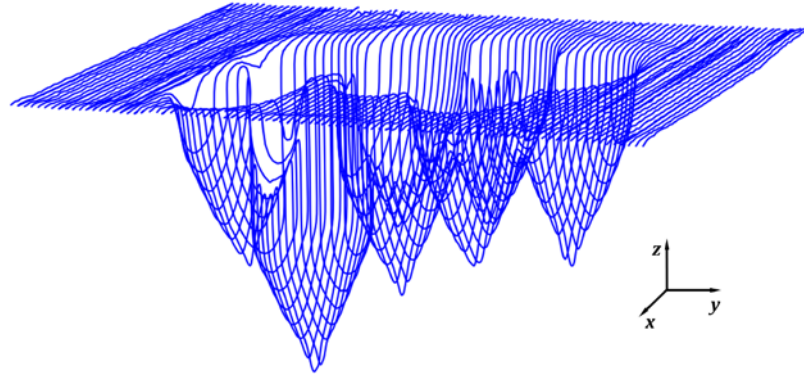
The coordinates of such points can be defined as follows:  $z_P$  and  $z_N$  were defined by finding the maximum z-coordinate on the damaged cross-section, which is  $z_T$  in Fig. 5b.  $z_Q$  and  $z_M$  were defined by exploring the minimum z-coordinate on the damaged cross-section, which is  $z_G$ . Since the damaged model was sliced along the y-axis,  $y_P = y_Q = y_M = y_N = y_S = y_E$ .  $x_P$  and  $x_N$  were randomly defined as long as  $x_P$  is much less than the minimum x-coordinate of the damaged points and  $x_N$  is much larger than the maximum x-coordinate of the damaged points. Once  $x_P$ ,  $x_N$  and the side wall inclination angle  $\theta$  were defined, the coordinates  $x_Q$  and  $x_M$  can be calculated according to Eq. (1).

$$\begin{cases} x_Q = \frac{z_P - z_Q}{\tan \theta} + x_P \\ x_M = x_N - \frac{z_N - z_M}{\tan \theta} \end{cases} \quad (1)$$

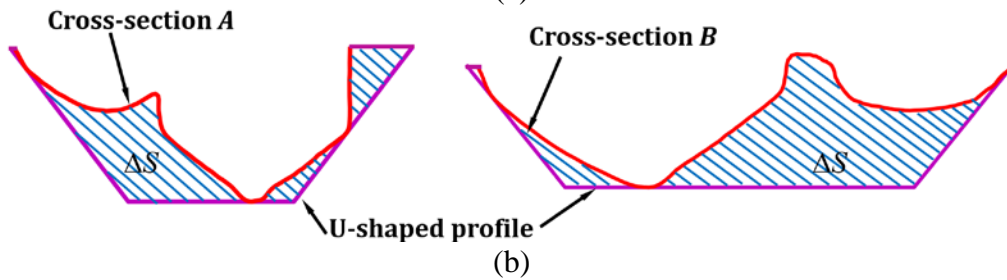
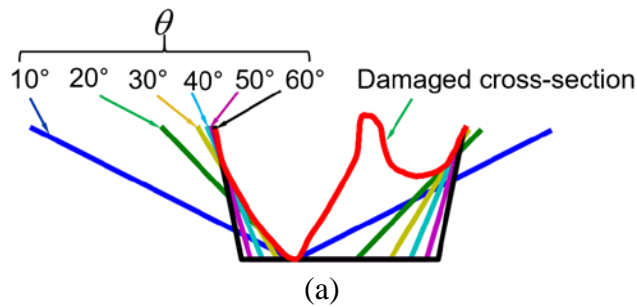
Once the two approaching lines were defined, relationship check between the approaching lines and the cross-section was conducted. If there is no intersection, a step was applied to  $x_P$  and  $x_N$  to make the approaching lines closer to the cross-section, and another checking iteration was conducted. Two approaching lines that firstly have intersections with the damaged curve can be obtained and lines before this iteration were gathered, which is shown in Fig. 5b. Finally, line  $PN$  and  $QM$  were added to close the U-shaped contour.

The inclination angle  $\theta$  of the two approaching lines can be operator determined and adjusted flexibly according to the specifications and performance of the LAM system. It should be noted that  $\theta$  has a significant effect on the cut-off volume that should be machined in the pre-repair machining step. A small  $\theta$  can give a good accessibility to the LAM system but may result in a much more cut-off volume. An optimized  $\theta$  needs to be determined which not only reveals good accessibility but also holds a minimized cut-off volume. For this purpose, a series of approaching lines with varied inclination angle was adopted to intersect a cross-section shown in Fig. 6a. Inclination angle  $\theta$  controls the accessibility and it shouldn't approach  $90^\circ$ . A series of experiments were conducted that aim to refill slots with different sidewall inclination angle on H13 tool steel and it was found that  $75^\circ$  tilt angle can still yield a sound bi-material bonding and good material properties. Therefore, the range of angle  $\theta$  was limited in  $[10^\circ, 75^\circ]$ . The area difference between the U-shaped profile and the cross-section,  $\Delta S$  shown in Fig. 6b, can indicate the cut-off area. A series of approaching lines were processed on cross-sections A and B as shown in Fig. 6a-b and the relationship between  $\Delta S$  and inclination angle  $\theta$  was plotted in Fig. 6c.

It was observed from Fig. 6c that for both cross-sections, the area  $\Delta S$  decreases and then increases with the increase of angle  $\theta$ . The curves indicate that neither a minimum or a maximum tilt angle can result in the minimum cut-off volume. It was found that the optimal angle  $\theta$  for CS A is  $26^\circ$  and is  $31^\circ$  for CS B. Therefore, the optimal angle  $\theta$  is highly dependent on the profile of the cross-section and should be determined for each cross-section. It can be found that for a very deep but thin damage, the minimum cut-off volume is nearly at angle  $90^\circ$ . This is because the closer of the angle to  $90^\circ$ , the less the cut-off will be.



**Fig. 5** Model slicing and enveloping boundary determination; (a) Cross-sections of the damaged block (layer thickness = 0.5 mm); (b) U-shaped enveloping boundary;



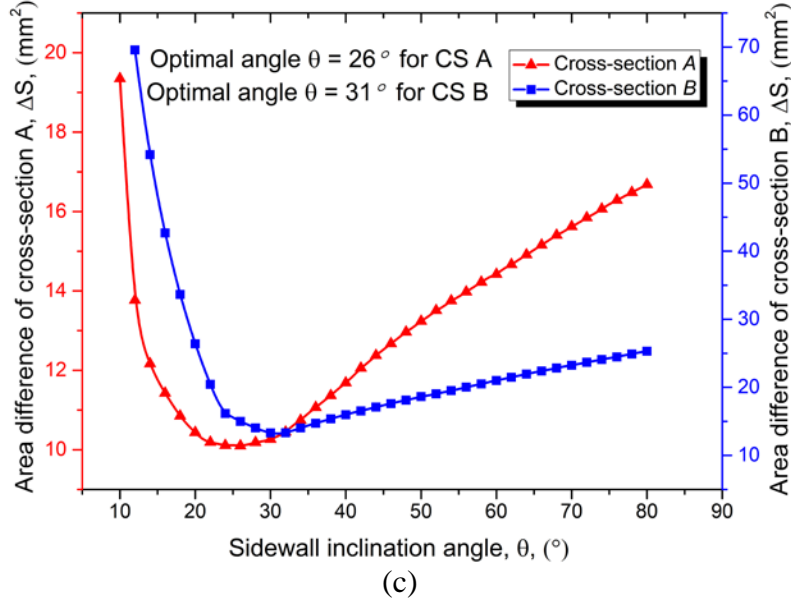


**Fig. 6** Sidewall inclination angle optimization for the U-shaped boundary. (a) U-shaped boundary with varied approaching lines; (b) U-shaped boundary for cross-sections A and B; (c) Relationship between area difference  $\Delta S$  and sidewall inclination angle  $\theta$

### 2.3.2 Convex-hull boundary definition

One can see in Fig. 5b that for U-shaped boundary, the bottom connecting line  $QM$  is parallel to the x-axis, and this may result in extra material cut-off in the polygon  $GMETG$ . This material over-cut comes worse when one deep defect is presented while majority defects are shallow. To further minimize cut-off volume, the convex-hull boundary was obtained as shown in Fig. 7a. The convex-hull of any polygon can be easily obtained based on existing algorithm [29]. However, one should notice that the convex-hull cannot be directly utilized as the boundary for pre-machining owing to the possibility of the steep area as shown in Fig. 7a. The line segments in those regions have big tangents that cannot guarantee the accessibility. Therefore, such lines need to be tilted. The algorithm for tilting lines with big tangent is schematically depicted in Fig. 7b and discussed below.

Suppose polygon  $P_i P_{i+1} \cdots P_{i+6} P_{i+7}$  is a convex-hull of one cross-section. The inclination angle of  $P_i P_{i+1}$  is indicated as  $\theta$ . Because  $\theta$  is beyond the allowed accessible angle,  $P_i$  needs to be rotated around  $P_{i+1}$  to  $P'_i$ . The coordinate of  $P'_i(x'_i, y'_i, z'_i)$  can be calculated according to Eq. 2, where  $(x_{i+1}, y_{i+1}, z_{i+1})$  is the coordinate of  $P_{i+1}$  and  $\gamma$  is the complementary angle of  $\theta$ . The inclination angle of  $P_{i+1} P_{i+2}$  also exceeds the allowed angle and therefore,  $P_{i+1}$  also needs to be rotated around  $P_{i+2}$  to  $P'_{i+1}$ . After that, the shifted polygon is  $P'_i P'_{i+1} \cdots P'_{i+6} P'_{i+7}$ . However, the inclination angle  $P'_i P'_{i+1}$  still surpasses the desired angle and therefore,  $P'_i$  needs to be further rotated around  $P'_{i+1}$  to  $P''_i$ . After the second iteration, the shifted polygon became  $P''_i P''_{i+1} \cdots P''_{i+6} P''_{i+7}$ . There is another iteration to move  $P''_{i+7}$  to  $P'''_{i+7}$ . Finally, the contour  $P'''_i P'''_{i+1} \cdots P'''_{i+6} P'''_{i+7}$  is obtained that satisfies the accessibility requirement, and therefore, can be used as a boundary for cut-off volume definition.



The aforementioned algorithm was applied to a cross-section as shown in Fig. 7a and the optimized contour is depicted in Fig. 7c. As illustrated in Fig. 7c, the steep area in the original convex hull was successfully tilted.

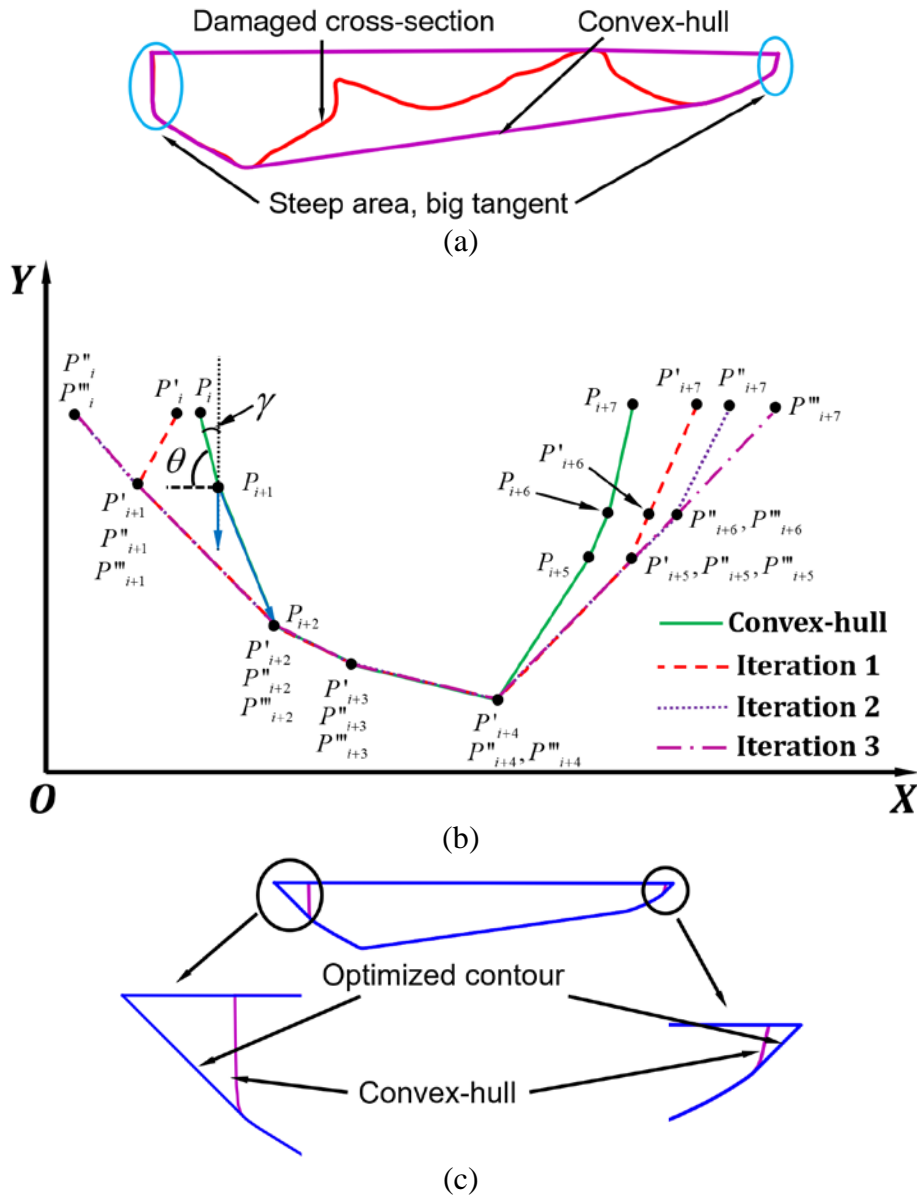


**Fig. 7** Convex-hull boundary definition. (a) Convex-hull processed on a cross-section; (b) Sidewall inclination angle optimization for convex-hull boundary; (c) Optimized contour

when  $y_{i+1} < y_i$  (Decreasing):

$$x_i' = x_{i+1} - \sqrt{\left(\frac{y_{i+1} - y_i}{\cos \gamma}\right)^2 - (y_{i+1} - y_i)^2}$$

$$y_i' = y_i$$

$$z_i' = z_i$$

when  $y_{i+1} > y_i$  (Increasing):

$$x_{i+1}' = x_i + \sqrt{\left(\frac{y_{i+1} - y_i}{\cos \gamma}\right)^2 - (y_{i+1} - y_i)^2} \quad (2)$$

$$y_i' = y_i$$

$$z_i' = z_i$$

## 2.4 Target geometry acquisition

U-shaped and convex-hull strategies were processed on the STL model with ball-indentations (Fig. 8a). For U-shaped strategy, side wall with fixed inclination angle  $\theta = 45^\circ$  and optimized angle were both conducted, and the target models were shown in Figs. 8b and 8c, respectively. The model processed using convex-hull strategy was presented in Fig. 8d.

The volume of the untreated damaged model (Fig. 8a) and volumes of processed models (Figs. 8b-d) using proposed strategies were summarized in Table 1. The volumes of machined models are different because the strategies for target geometry acquisition are different. It can be observed from Table 1 that the U-shaped strategy with optimized sidewall inclination angle will machine off less material compared with non-optimized U-shaped strategy. However, convex-hull strategy results in the least amount of cut-off volume, which is expected. Therefore, in the next machining step, convex-hull strategy-generated geometry was adopted as the guide model for machining toolpath and NC code generation.

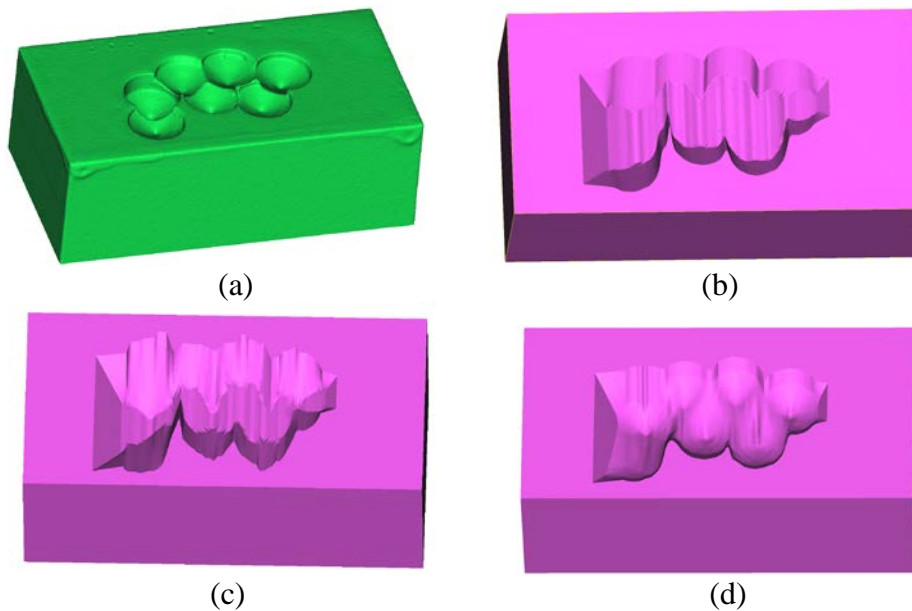


**Fig. 8** Untreated and processed models; (a) Model of the damaged substrate; Model pre-machined using U-shaped strategy (b), U-shaped strategy with optimized sidewall inclination angle (c) and convex-hull strategy (d)

**Table 1** Volume of the model with varied pre-machining strategies

Model	Damaged	U-shaped machined	U-shaped machined with optimized sidewall angle	Convex-hull machined
Volume (mm <sup>3</sup> )	22245.1	21216.3	21251.6	21331.8
Cut-off volume (mm <sup>3</sup> )	-	1028.8	993.5	913.3

## **2.5 Pre-repair machining program generation and pre-machining**

Once the target geometry was obtained, it was loaded to Mastercam software to generate the machining toolpath (Fig. 9a) and program. The milling parameters are listed in Table 2. The damaged substrate was clamped on a fixture and machined on a Fryer MC-30 with the setup shown in Fig. 9b. The machined part is shown in Fig. 9c.

**Table 2** Pre-repair machining parameters for surface impact damage

Tool	Feed rate	Spindle speed	Stepdown	Stepover percentage	Toolpath type
1/4" ball-end mill	508 in/min	2000 r/min	0.5	33 %	High-speed spiral

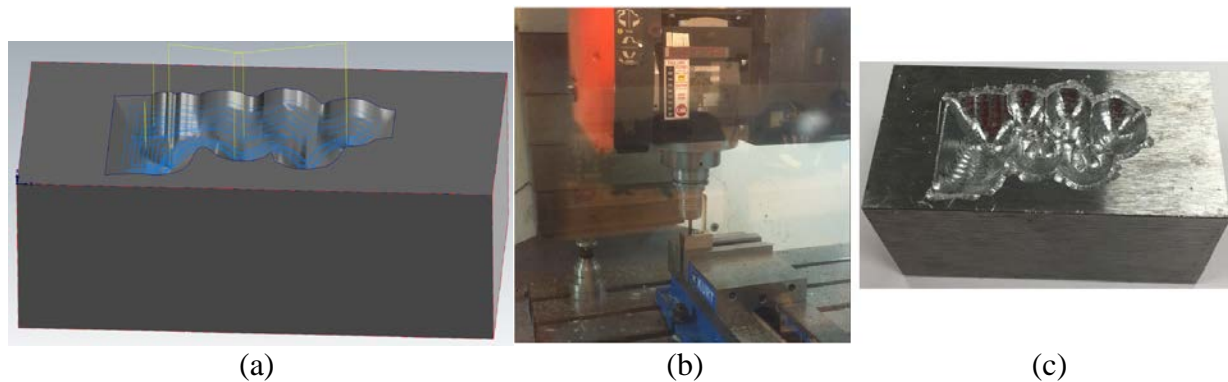


**Fig. 9** Pre-machining toolpath (a), experiment setup (b) and machined substrate (c)

## **3. Pre-repair machining strategy for surface erosion, wear and corrosion**

Casting dies are subjected to rapid heating and cooling cycles during their service that causes dimensional distortion and cracking. In addition, frequently contacting with casting alloys such as liquid aluminum alloys causes surface defects such as erosion, wear, and corrosion. It is reported that thermal fatigue and erosion are major contributions to the failure of casting dies [30]. Die surface flaws destruct the quality of casted copies, therefore needs frequent scheduled repair.

Directly depositing materials on damaged die surfaces is not suggested because of the following reasons. Firstly, damaged surface usually contains impurities such as oxidized and contaminated materials. Surface pitting may also cause numerous tiny localized defects. Coating materials on such untreated surfaces cannot guarantee the solid bi-material bonding which may cause unpredictably delamination during application. Secondly, LAM requires a certain surface roughness for material deposition (shiny surface requires high laser power and rough surface requires lower laser power). Damaged surfaces may not have a constant, defined roughness, whereas a machined surface can provide this. Fortunately, such surface defects are usually superficial and can be easily removed by cutting off a thin layer of material from the target surface. The thickness of machined material can be determined as long as the machined surface is defect-free. Once such layer is machined, material can be coated on such region to reobtain the designed geometry.

The current research proposes a general procedure for treating surfaces with erosion, wear, and corrosion. In general, the damaged component is 3D scanned to recreate its STL model. After that, the model is loaded to CAM software, and the target regions are selected. Machining parameters including cut-off thickness are determined and machining program is generated. Subsequently, the program is transferred to CNC for pre-machining. The following sections detailed the pre-repair machining procedure for such damage.

### **3.1 Model reconstruction of a casting die with surface defects**

A casting die shown in Fig. 10a has damaged regions on its working convex area that dominated by tiny rough surfaces. In order to machine off a thin layer of material from the part, the STL model of the die was generated using the configuration in Fig. 3 and the recreated model is shown in Fig. 10b. It should be pointed out that creating the model of the whole part is not necessary for pre-repair machining. This is because only the surface with defects needs to be targeted and other regions will not be treated. Generating the whole model not only dramatically slow down the 3D scanning process, especially for a large complex structure, but also sophisticate the toolpath generating process due to the large size of the imported model.

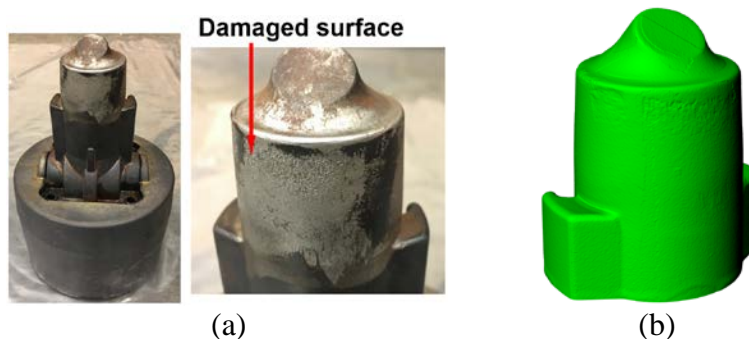


**Fig. 10** (a) A casting die with surface erosion, wear, and corrosion; (b) STL model of the damaged region of the casting die

### **3.2 Machining volume determination, program generation, and pre-machining**

The volume of materials that need machining depends on the depth of surface defects. The defects of surface erosion, wear and corrosion are usually superficial and can be effectively removed through one pass machining. The cut depth for machining can be determined based on the condition of damaged components. For the casting die in Fig. 10a, materials with 0.5 mm layer thickness were machined. The toolpath was generated as shown in Fig. 11a and the simulated machined part is shown in Fig. 11b.

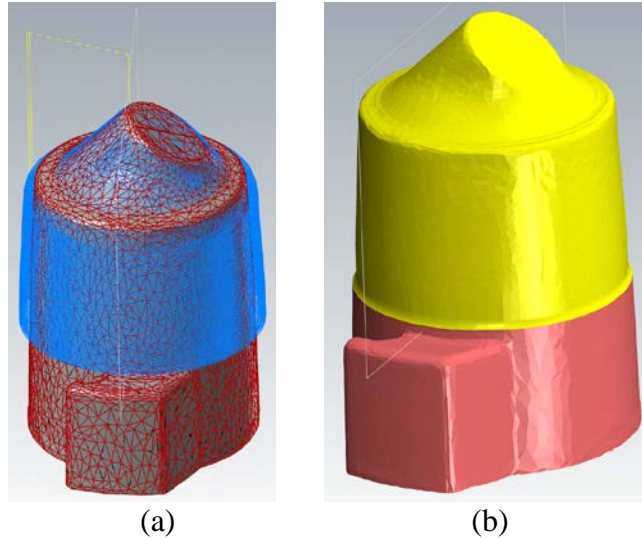


**Fig. 11** (a) Pre-machining tool path generation; (b) Pre-machined model of the die

#### **4. Pre-repair machining strategy for cracking**




The heating and cooling cycles during metal casting cause cyclic compressive and tensile stress conditions which led to thermal fatigue to the casting die [31]. That is why H13 hot work tool steel is usually adopted as die material owing to its high hardenability and good thermal fatigue resistance. Thermal fatigue cracking is a common failure in die-casting dies and engine blades after thousands of shots. The cracking is first to like to appear at corners and edges with small radius [32].

Detailed machining procedure for cracking highly depends on the appearance of cracks and can be determined only after considering a number of factors, such as the depth and length of cracks, surrounding structures, accessibility of cracks to machining tool and LAM system, surface or internal cracking, etc. Therefore, this paper presents some candidate machining approaches that can be considered for cracking removal.

Table 4 lists a few machining methods for cracking. Cracks are classified into shallow and deep cracks because they may need different machining methods. For example, for shallow cracks, they can be easily and effectively removed by surface grinding. Therefore, 3D scanned models of such parts are not needed. For deep cracks, Electro discharge machining (EDM) and CNC (computerized numerical control) machining can be utilized. EDM can cut off materials with cracks much more efficiently, but it is only applicable to cracks that can be accessible to EDM wire. If the cracking is surrounded by other structures, EDM is not applicable and therefore, CNC machining can be considered. Such machining procedures will consume more material over surface grinding. One should know that internal cracking is not easy to observe visually and then may require nondestructive testing. Once the internal cracking is located, a slot can be made to remove the cracks. However, machining a slot is not always working because a very deep slot is difficult to refill, especially when the edge of the slot is near vertical. In such cases, the U-shaped strategy can be applied or the portion of the component with cracks can be completely cut-off and rebuild. This approach is applicable to any cracks regardless of depth, but it will cut-off a huge amount of material. Therefore, one needs to evaluate the cost by repairing them over replacement

with a new copy. In this paper, a titanium engine blade with cracks was machined using EDM to show the machining procedure.

**Table 4** Candidate machining approaches for cracking

Cracking depth	Machining method	Machining overview	Cut-off material	Remarks
Shallow	Grinding	Cracking removal by grinding 	Small	Applicable to surface cracking. Convex grinding wheel for good accessibility
Deep	EDM (Electro-discharge machining)	Cracking removal using EDM 	Moderate	Applicable to cracks that are accessible to EDM wire
	CNC machining	Cracking removal using CNC 		Applicable to cracks that are accessible to cutting tools
	Cracking piece replacement	Cut off the portion that has cracks. Rebuild the cut-off part for replacement	Large	Applicable to all cracks regardless of depth

#### **4.1 Pre-repair machining strategy for cracking**

An engine blade was utilized to demonstrate the pre-repair machining strategy for cracking. Trailing edge cracking is a common failure in turbine or compressor blade mainly due to excessive stress, overloading, overheating or defective materials. Several studies have been targeting on blade repair, mainly focusing on damage extraction [18], [33], [34], material deposition process [35]–[37] and repair automation [38], [39], while no reporting on strategies of pre-machining. It is required to cut off the material surrounding cracks because non-machined cracks give no accessibility to LAM system, as shown in Fig. 12a. This is why the defects in blade edge reported in [19], [38], [40] have U or V-shaped geometry.

To perform pre-machining, the blade as shown in Fig. 12a was digitally scanned to acquire its 3D model as shown in Fig. 12b. After that, the defective area was selected as shown in Fig. 12c. By selecting the damaged area, the points located at the worn domain can be easily extracted which is shown in Fig. 13a, and subsequently, the convex hull of the point set was obtained. It should be pointed out that the convex hull cannot be directly used for pre-machining because the bottom portion of the convex hull blocks the accessibility. In order to create an open V-shaped geometry, the line segments of the convex hull were tilted according to the algorithm illustrated in 2.3.2. The maximum sidewall inclination angle  $\theta$  is limited at  $60^\circ$ . The finally optimized contour was shown in Fig. 13b. EDM wire then follows the optimized contour for pre-machining and the pre-machined blade is shown in Fig. 13c.

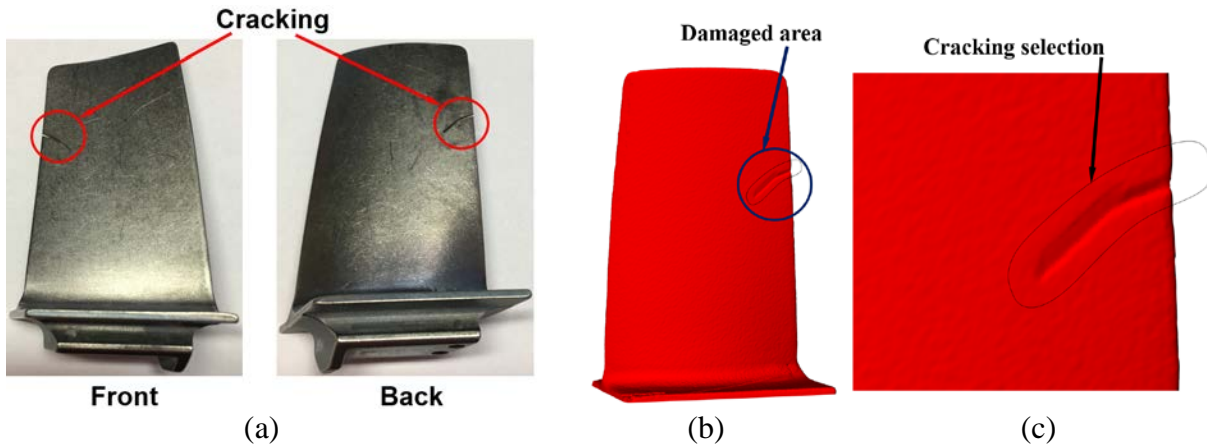


**Fig. 12** (a) Titanium blade with cracks; (b) Reconstructed model of the blade; (c) Selection of points located at the damaged area

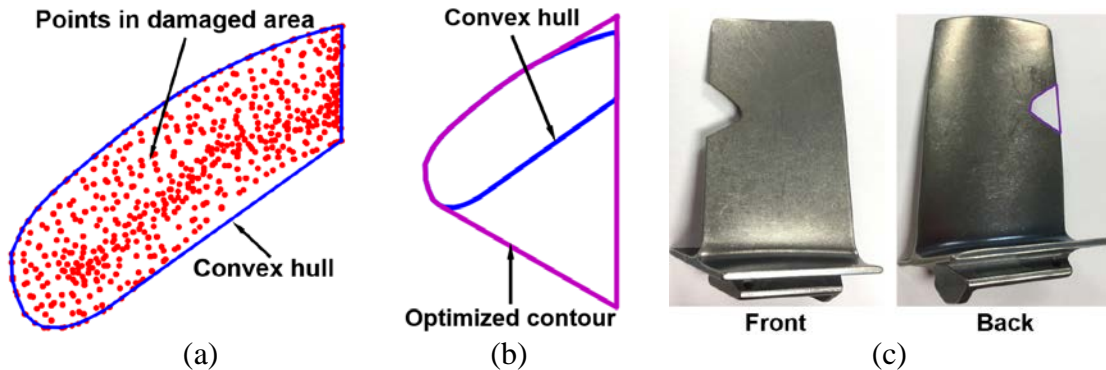


**Fig. 13** (a) Damaged point set extraction and its convex hull; (b) Optimized contour; (c) Blade after pre-machining

## **5. Conclusion**

Pre-repair machining of damaged components is crucial before additive manufacturing to make sure the damage is accessible and the substrate is free of contamination. For this purpose, this paper presents several pre-machining strategies targeting at surface defects and cracking. Damaged part was first inspected and machining tool was determined. Reconstructed model of the damage component is usually required for pre-repair machining toolpath generation. For surface impact defects, two strategies, U-shaped, and Convex-hull strategies were introduced for cut-off volume definition. The convex-hull method results in less material removal and is, therefore, preferred. For surface erosion, wear, and corrosion, a thin layer of material at the damaged region was removed to get rid of contaminated layers or numerous tiny defects. Approach for removing cracking should be determined after considering several factors such as the depth and length of cracks, surrounding structures, accessibility of cracks, surface or internal cracking, etc. This study presents an approach for removing cracks in blade edge using wire-EDM.

## Acknowledgment

This project was supported by TOYOTA/Bodine Aluminum, National Science Foundation Grants CMMI-1547042 and CMMI-1625736, and the Intelligent System Center, Center for Aerospace Manufacturing Technology, and Material Research Center at Missouri S&T. Their financial support is greatly appreciated.

## Reference

- [1] R. Raju, M. Duraiselvam, V. Petley, S. Verma, and R. Rajendran, "Microstructural and mechanical characterization of Ti6Al4V refurbished parts obtained by laser metal deposition," *Mater. Sci. Eng. A*, vol. 643, pp. 64–71, 2015.
- [2] K. Zhang, S. Wang, W. Liu, and X. Shang, "Characterization of stainless steel parts by Laser Metal Deposition Shaping," *Mater. Des.*, vol. 55, pp. 104–119, 2014.
- [3] E. Brandl, B. Baufeld, C. Leyens, and R. Gault, "Additive manufactured Ti-6Al-4V using welding wire: Comparison of laser and arc beam deposition and evaluation with respect to aerospace material specifications," *Phys. Procedia*, vol. 5, no. PART 2, pp. 595–606, 2010.
- [4] W. Li, X. Chen, L. Yan, J. Zhang, X. Zhang, and F. Liou, "Additive manufacturing of a new Fe-Cr-Ni alloy with gradually changing compositions with elemental powder mixes and thermodynamic calculation," *Int. J. Adv. Manuf. Technol.*, vol. 95, no. 1, pp. 1013–1023, Mar. 2018.
- [5] W. Li, L. Yan, X. Chen, J. Zhang, X. Zhang, and F. Liou, "Directed energy depositing a new Fe-Cr-Ni alloy with gradually changing composition with elemental powder mixes and particle size' effect in fabrication process," *J. Mater. Process. Technol.*, vol. 255, pp. 96–104, 2018.
- [6] W. Cui, X. Zhang, and F. Liou, "Additive Manufacturing of High-Entropy Alloys CE A Review," *Solid Free. Fabr. Symp.*, pp. 712–724, 2017.
- [7] R. M. Mahamood and E. T. Akinlabi, "Laser metal deposition of functionally graded Ti6Al4V/TiC," *Mater. Des.*, vol. 84, pp. 402–410, 2015.
- [8] G. P. Dinda, A. K. Dasgupta, and J. Mazumder, "Laser aided direct metal deposition of Inconel 625 superalloy: Microstructural evolution and thermal stability," *Mater. Sci. Eng. A*, vol. 509, no. 1, pp. 98–104, 2009.
- [9] X. Zhang, W. Li, X. Chen, W. Cui, and F. Liou, "Evaluation of component repair using direct metal deposition from scanned data," *Int. J. Adv. Manuf. Technol.*, Dec. 2017.
- [10] X. Zhang, W. Li, K. M. Adkison, and F. Liou, "Damage reconstruction from tri-dexel data for laser-aided repairing of metallic components," *Int. J. Adv. Manuf. Technol.*, Mar. 2018.
- [11] J. Gao, X. Chen, O. Yilmaz, and N. Gindy, "An integrated adaptive repair solution for complex aerospace components through geometry reconstruction," *Int. J. Adv. Manuf. Technol.*, vol. 36, no. 11–12, pp. 1170–1179, 2008.
- [12] H. Qi, M. Azer, and P. Singh, "Adaptive toolpath deposition method for laser net shape manufacturing and repair of turbine compressor airfoils," *Int. J. Adv. Manuf. Technol.*, vol. 48, no. 1–4, pp. 121–131, 2010.
- [13] X. Penaranda, S. Moralejo, A. Lamikiz, and J. Figueras, "An adaptive laser cladding methodology for blade tip repair," *Int. J. Adv. Manuf. Technol.*, vol. 92, no. 9, pp. 4337–



- 4343, Oct. 2017.
- [14] J. Bennett, R. Dudas, J. Cao, K. Ehmann, and G. Hyatt, "Control of heating and cooling for direct laser deposition repair of cast iron components," in *2016 International Symposium on Flexible Automation (ISFA)*, 2016, pp. 229–236.
  - [15] W. Li, J. Zhang, X. Zhang, and F. Liou, "Effect of Optimizing Particle Size on Directed Energy Deposition of Functionally Graded Material with Blown Pre-mixed Multi-powder," 2017.
  - [16] W. Li, X. Zhang, and F. Liou, "Modeling analysis of argon gas flow rate's effect on pre-mixed powder separation in laser metal deposition process and experimental validation," *Int. J. Adv. Manuf. Technol.*, vol. 96, no. 9, pp. 4321–4331, Jun. 2018.
  - [17] W. Wang, A. J. Pinkerton, L. M. Wee, and L. Li, "Component Repair Using Laser Direct Metal Deposition," in *Proceedings of the 35th International MATADOR Conference*, 2007, pp. 345–350.
  - [18] X. Zhang, W. Li, and F. Liou, "Damage detection and reconstruction algorithm in repairing compressor blade by direct metal deposition," *Int. J. Adv. Manuf. Technol.*, vol. 95, no. 5, pp. 2393–2404, Mar. 2018.
  - [19] X. Zhang, W. Li, W. Cui, and F. Liou, "Modeling of worn surface geometry for engine blade repair using Laser-aided Direct Metal Deposition process," *Manuf. Lett.*, vol. 15, pp. 1–4, 2018.
  - [20] T. Petrat, B. Graf, A. Gumenyuk, and M. Rethmeier, "Laser Metal Deposition as Repair Technology for a Gas Turbine Burner Made of Inconel 718," *Phys. Procedia*, vol. 83, pp. 761–768, 2016.
  - [21] P. Kattire, S. Paul, R. Singh, and W. Yan, "Experimental characterization of laser cladding of CPM 9V on H13 tool steel for die repair applications," *J. Manuf. Process.*, vol. 20, pp. 492–499, 2015.
  - [22] J. M. Wilson, C. Piya, Y. C. Shin, F. Zhao, and K. Ramani, "Remanufacturing of turbine blades by laser direct deposition with its energy and environmental impact analysis," *J. Clean. Prod.*, vol. 80, pp. 170–178, 2014.
  - [23] K. Eiamsa-ard, H. J. Nair, L. Ren, J. Ruan, T. Sparks, and F. W. Liou, "Part Repair using a Hybrid Manufacturing System," *16th Solid Free. Fabr. Symp. SFF 2005*, pp. 425–433, 2005.
  - [24] C. Bremer, "Automated Repair and Overhaul of Aero-Engine and Industrial Gas Turbine Components," no. 4725X. pp. 841–846, 2005.
  - [25] J. Gao, X. Chen, O. Yilmaz, and N. Gindy, "An integrated adaptive repair solution for complex aerospace components through geometry reconstruction," *Int. J. Adv. Manuf. Technol.*, vol. 36, no. 11, pp. 1170–1179, Apr. 2008.
  - [26] O. Yilmaz, N. Gindy, and J. Gao, "A repair and overhaul methodology for aeroengine components," *Robot. Comput. Integr. Manuf.*, vol. 26, no. 2, pp. 190–201, 2010.
  - [27] X. Zhang, W. Li, K. M. Adkison, and F. Liou, "Damage reconstruction from tri-dexel data for laser-aided repairing of metallic components," *Int. J. Adv. Manuf. Technol.*, pp. 1–14, 2018.
  - [28] J. M. Wilson, C. Piya, Y. C. Shin, F. Zhao, and K. Ramani, "Remanufacturing of turbine blades by laser direct deposition with its energy and environmental impact analysis," *J. Clean. Prod.*, vol. 80, pp. 170–178, Oct. 2014.
  - [29] J. Sklansky, "Finding the Convex Hull of a Simple Polygon," *Pattern Recogn. Lett.*, vol. 1, no. 2, pp. 79–83, Dec. 1982.

- [30] S.-H. Chang, T.-P. Tang, Y.-C. Chen, and J.-K. Chen, "Enhancement of Erosion Resistance on AISI H13 Tool Steel by Oxynitriding Treatment," *ISIJ Int.*, vol. 49, no. 3, pp. 421–424, 2009.
- [31] A. Persson, S. Hogmark, and J. Bergström, "Failure modes in field-tested brass die casting dies," *J. Mater. Process. Technol.*, vol. 148, no. 1, pp. 108–118, 2004.
- [32] Z. X. Jia, J. Q. Li, L. J. Liu, and H. Zhou, "Performance enhancements of high-pressure die-casting die processed by biomimetic laser-remelting process," *Int. J. Adv. Manuf. Technol.*, vol. 58, no. 5–8, pp. 421–429, 2012.
- [33] Y. Rong, J. Xu, and Y. Sun, "A surface reconstruction strategy based on deformable template for repairing damaged turbine blades," *Proc. Inst. Mech. Eng. Part G J. Aerosp. Eng.*, vol. 228, no. 12, pp. 2358–2370, 2014.
- [34] J. Gao, X. Chen, D. Zheng, O. Yilmaz, and N. Gindy, "Adaptive restoration of complex geometry parts through reverse engineering application," *Adv. Eng. Softw.*, vol. 37, no. 9, pp. 592–600, 2006.
- [35] G. Bi and A. Gasser, "Restoration of Nickel-Base Turbine Blade Knife-Edges with Controlled Laser Aided Additive Manufacturing," *Phys. Procedia*, vol. 12, pp. 402–409, 2011.
- [36] S. Nowotny, S. Scharek, E. Beyer, and K.-H. Richter, "Laser Beam Build-Up Welding: Precision in Repair, Surface Cladding, and Direct 3D Metal Deposition," *J. Therm. Spray Technol.*, vol. 16, no. 3, pp. 344–348, Sep. 2007.
- [37] M. Gäumann, C. Bezençon, P. Canalis, and W. Kurz, "Single-crystal laser deposition of superalloys: processing–microstructure maps," *Acta Mater.*, vol. 49, no. 6, pp. 1051–1062, 2001.
- [38] J. Gao, X. Chen, O. Yilmaz, and N. Gindy, "An integrated adaptive repair solution for complex aerospace components through geometry reconstruction," *Int. J. Adv. Manuf. Technol.*, vol. 36, no. 11, pp. 1170–1179, Apr. 2008.
- [39] J. Gao, J. Folkes, O. Yilmaz, and N. Gindy, "Investigation of a 3D non-contact measurement based blade repair integration system," *Aircr. Eng. Aerosp. Technol.*, vol. 77, no. 1, pp. 34–41, 2005.
- [40] T. Blades, "Detc2011-48652 Virtual Repair : Geometric Reconstruction for Remanufacturing Gas," *Cross Sect.*, pp. 1–10, 2011.